VI International Conference on Computational Bioengineering
ICCB 2015
M. Cerrolaza and S.Oller (Eds)

IVUS IMAGE CONDITIONING FOR IN-VIVO CHARACTERIZATION OF ARTERIAL TISSUE

GONZALO D. MASO TALOU [‡,†,*], JORGE M. PÉREZ ZERPA [º], PABLO J. BLANCO[‡,†], ALFREDO CANELAS [º] AND RAÚL A. FEIJÓO[‡,†]

[‡] Laboratório Nacional de Computação Científica (LNCC/MCTI)
Av. Getúlio Vargas 333, 25651075 Petrópolis, Brazil
e-mail: {gonzalot,pjblanco,feij}@lncc.br, web page: http://www.lncc.br

[†] Instituto Nacional de Ciência e Tecnologia em Medicina Assistida por Computação Científica
Av. Getúlio Vargas 333, 25651075 Petrópolis, Brazil
e-mail: {gonzalot,pjblanco,feij}@lncc.br, web page: http://macc.lncc.br/

[º] Instituto de Estructuras y Transporte, Facultad de Ingeniería
Universidad de la República
Julio Herrera y Reissig 565, 11300 Montevideo, Uruguay
e-mail: {jorgepz,acanelas}@fing.edu.uy, web page: http://www.fing.edu.uy/iet

Key words: Tissue Characterization, IVUS, Medical Imaging

Abstract. In-vivo characterization of arterial tissue is of paramount importance for culprit plaque identification, patient risk assessment and surgical planning. As culprit plaque histology is well known, the in-vivo tissue composition could be a valuable diagnostic and therapeutic tool. Currently, no in-vivo imaging technique provides direct histological information of the vessel wall. Different IVUS processing techniques have been used to infer the tissue composition from acoustic impedance variations. Most popular approaches for plaque characterization are based on classification schemes trained with ex-vivo tissue samples, which may lead to mischaracterization due to post-mortem changes in tissue properties. Hence, pure image based techniques are not capable of delivering the internal stress state of the vessel wall, which are consequence of strains produced by pressure loads. However, these images, under proper conditioning, provide fully detailed information about the wall kinematics, such as strains and rigid motions.

In this manuscript we will present the necessary steps in IVUS image processing to have at hand well-conditioned data to accurately identify the wall kinematics and thus formulate a inverse problem to characterize arterial wall mechanical properties. The first step consists in the IVUS gating to extract different cardiac phases. Then, registration algorithms aim at removing transversal rigid motions. The so conditioned images are the input to different optical flow algorithms with the aim of describing the wall kinematics, that is, displacement vector field throughout the entire IVUS image. This displacement field is employed as input data for the inverse mechanical problem in which the material parameters of a constitutive model are determined by solving a nonlinear optimization problem.

The focus of this work is on the conditioning stages of the IVUS images and the performance of optical flow algorithms in recognizing the displacement field. Concerning the inverse

characterization, preliminary results will be presented using a state-of-the-art formulation of the optimization problem.

1 INTRODUCTION

In-vivo tissue characterization of coronary arteries is of paramount importance for culprit plaque identification. Several works have identified the histological characteristics of culprit plaque [1, 2], although reliable diagnostic techniques for tissue composition description are still missing in medical practice. Promissory solutions for this open problem are the image-based tissue characterization [3-5] and the elastographies [6-8].

Image-based characterizations are low invasive techniques that analyze the acoustic impedance variations presented in the IVUS study. Although, these solutions rely in classification schemes that label in-vivo tissues based on data extracted from ex-vivo samples. This hypothesis is not necessarily valid due to the biochemical and structural variation of the vessel wall tissues after host decease, as well as, due to the not completely accurate in-vitro approximations to reproduce the in-vivo conditions [9]. Also, different strategies based on these ideas may not reach consensus on lipidic tissue identification [10].

Elastographies estimate the vessel wall tissues properties that are compatible with the tissue kinematics along the cardiac cycle. The main difficulty for these approaches is the accurate estimation of local tissue displacements between different cardiac phases. Since the transducer migrates periodically due cardiac contractions, the transversal and axial registration of the structures is mandatory for the appropriate displacement estimation. Most elastography techniques addresses transversal registration only, neglecting axial displacements of the transducer which may introduce spatial inconsistencies between the compared structures [11].

The present article proposes an IVUS study preprocessing methodology for tissue characterization schemes based on the analysis of the wall kinematics. Here, the IVUS study is subdivided by cardiac phases to achieve time consistent image sequences of the vessel. To identify the frames among sequences that correspond to the same spatial position, an axial and transversal registration process is performed. Then, a multi-resolution optical flow technique is applied to estimate the displacement vector field throughout the IVUS images that correspond to different cardiac phases at a specific vessel location. Finally, a formulation for material property identification is presented and applied on top of the displacement fields provided by the optical flow technique.

It is worthwhile to mention that the presented methodology uses standard IVUS studies (no study radiofrequencies are required), enabling its application to retrospective medical studies.

2 METHODOLOGY

To consistently perform tissue characterization, it is assumed that the same vessel transversal area must be given at two different loading states (i. e. at different cardiac phases). To that end, an IVUS gating scheme is performed to identify the cardiac phase at each frame. Furthermore, cardiac contraction imprints a transducer displacement from phase to phase hindering frame selection at the same axial position of the vessel, as well as, the alignment of the vessel wall structures. To underpin these issues, a registration process identifies the pair of frames at two different cardiac phases that correspond to the same axial location and, then, align its structures.

The next step consists in the registration of the displacement field at the vessel wall to

properly characterize the kinematics for the material parameter estimation problem. An optical flow (OF) technique is a natural solution for this problem given that structures within the vessel wall maintain their intensity from frame to frame. To deal with displacements of more than one pixel the multi-resolution technique presented in [12] is employed, where velocity field estimations are performed at different frame resolutions, detecting, from lower to higher, the modal components of the velocity field.

Finally, we estimate the material parameters of a linear elastic constitutive model for the given displacement field. The constitutive model assumed for the material is isotropic linear elastic, as in [13]. The material parameters identification is performed through the formulation of an inverse problem. Recently, several strategies have been proposed for this kind of problem [14], however we consider a technique based on the Error in the Constitutive Equation (ECE) which has proven to be appropriate for material identification fed by full field measurements [15]. The inverse problem is solved through the application of an optimization procedure as it is done in [16].

2.1 IVUS gating

The gating phase is addressed in two different ways: using a full manual detection of the R-wave peak or using an image based gating method [17-19]. The first strategy can only be applied when the IVUS study is acquired synchronously with the ECG signal. The advantage of this approach is the robustness and reliability on the cardiac phase extraction. The second method is user independent and faster. The main disadvantage of these methods is the lack of robustness for patients with arrhythmia or in presence of infarcted vessel areas.

For this work, we choose to use the manual approach to obtain a more accurate phase extraction. In that process, the R-wave peaks is carried on by a specialist that indicates in a computer ECG viewer the R-wave peaks times. As the ECG signal is synchronously acquired with the IVUS study, we use the specialist indicated times to extract the frames associated with R-wave peak phase. Intra-observer and inter-observer variability of the manual gating is below 1 frame which gives a high confidence in the phase extraction process.

Once the R-wave peak phase is extracted, we pick the 7 frames before and the 7 frames after each R-wave peak frame to conform the 7 previous and 7 posterior phases to the R-wave peak phase. From these 15 phases of the cardiac cycle, we name as steadiest phase to the phase that minimizes the following cost functional

$$\Im_{st} = \underset{P_i, i\in[1,15]}{\operatorname{argmin}} \sum_{j=1}^{N_{P_i}} \sum_{x=1}^{W} \sum_{y=1}^{H} \left| \nabla I_j^{P_i}(x,y) \right| \tag{1}$$

where P_i is the i-th cardiac phase, $I_j^{P_i}$ the j-th frame of the cardiac phase P_i, N_{P_i} is the number of frames of the cardiac phase P_i in the IVUS study, W and H are the width and height of each IVUS frame.

2.2 Registration

By analyzing the steadiest phase, we select a frame (or group of frames) where we are interested to characterize the arterial tissue (e.g., stenosed regions or stent places). To perform

the characterization, we must pick the same spatial cross-section at the previous extracted phases, constructing a set of frames, S, that describes the kinematics of the vessel wall along the cardiac cycle. However, note that the rigid motion imprinted from the heart beating causes misalignment of the vessel wall structures along the cardiac phases. Then, a registration of the frames in the set S is performed to align the structures of interest.

To ensure that the same cross-section is picked from each cardiac phase, we perform an axial registration process. In this process, we search for the frame in each phase with minimum normalized cross-correlation against the frame of interest in the $\Im_{st}$ phase. As the transducer axial displacement is reported in the range of 1.5 ± 0.8 mm [11], then we search only in a neighborhood of 7 frames from N, where N is the frame position at the $\Im_{st}$ phase.

Posteriorly, in the transversal registration, we use the frame of the $\Im_{st}$ phase (steadiest frame) as reference to align the remaining phases frames in S. Particularly, to achieve the registration of the frame $I_j^{P_i}$, we must apply the rigid motion Ξ, composed by a rotation and a translation, such that maximizes

$$\Xi = \max_{\Xi' \in \mathcal{U}} c\left(I_j^{\Im_{st}}, I_j^{P_i}\left(x(\Xi'), y(\Xi')\right)\right) \tag{2}$$

where $\mathcal{U}$ is the space of admissible rigid movements, $x(\Xi'), y(\Xi')$ are the modified coordinates of $I_j^{P_i}$ after applying the rigid motion Ξ' over the frame and c is the normalized cross-correlation between two images. Note that since $I_j^{P_i}(x, y)$ is a discrete and limited in range, we define as admissible translations in $\mathcal{U}$ only displacements multiples of 1 pixel. Similarly, as the transducer performs 256 equally rotated scan lines per frame, we define as admissible rotations in $\mathcal{U}$ the multiples of 360/256 degrees.

As the functional defined by c over $\mathcal{U}$ in Equation (2) is usually non-convex and $\mathcal{U}$ is relatively small, we solve the maximization problem with a brute force approach.

2.3 Optical flow estimation

Once the set of frames S is aligned by the registration process, we estimate the displacement field between the frames of successive cardiac phases. The optical flow method adopted for this task is the multi-resolution approach presented in [12] due to its capabilities of: i) controlling the regularization through a non-linear weighting scheme; ii) estimating non-infinitesimal displacements; iii) dealing with high frequency noise by the combined local/global optimization. In that manner, we estimate the displacement vectorial field $U(x, y) = \left(u(x, y), v(x, y)\right)$ as

$$U = \sum_{n=1}^{N_S} \delta U^n \tag{3}$$

where N_S is the largest displacement in pixels that the methods recognize, δU^n is the n-th order component of the displacement field associated with a wavelength of $2^{N_S - n}$ pixels. Each δU^n component is calculated after the lower order components (i.e. $\delta U^i, i < n$) by solving the optimization problem presented as follows

$$\delta U^n = \min_{(\delta u^n, \delta v^n)} \int_{[0,T]} \int_{\Omega} [\psi_1 \left((\delta u^n, \delta v^n, 1)^T J_\rho * (DI^n \cdot (DI^n)^T) \, (\delta u^n, \delta v^n, 1) \right) + \gamma \psi_2 (|D(u^n + \delta u^n, v^n + \delta v^n)|^2) \,] \, d\Omega \, \mathrm{dt} \tag{4}$$

where $I^n = I(x + u^n, y + v^n)$, γ is a weight associated to the regularization term, J_ρ is the Gaussian kernel with ρ standard deviation, $D = \left(\frac{\partial}{\partial x}, \frac{\partial}{\partial y}, \frac{\partial}{\partial t} \right)^T$, $U^n = (u^n, v^n) = \sum_{m=1}^{n} (\delta u^m, \delta v^m)$ and $\psi_i(a) = 2\beta_i^2 \sqrt{1 + \frac{a}{\beta_i^2}}$.

2.4 Material parameters estimation

Let us consider an elastic body Ω composed by an isotropic linear elastic material, subjected to Dirichlet and Neumann boundary conditions. It is assumed that the displacements in that body, U, are measured in the whole region Ω (full-field-measurements FFM). Then, the material identification problem consists of the determination of the mechanical properties of the solid using this displacement field. In general the material is characterized by the constitutive tensor $\boldsymbol{C}$, however in this work we will estimate only the spatial distribution of the Young modulus E. The Poisson ratio is considered known.

The material identification problem is formulated as an optimization problem given by the minimization of the following cost functional

$$\min_{E \in \mathcal{V}_E} \mathcal{J}(E) + \alpha \mathcal{R}(E) \tag{5}$$

where $\mathcal{J}$ is a smooth error functional, $\mathcal{R}$ is a regularization term, α is the regularization coefficient and $\mathcal{V}_E$ is the set of admissible Young modulus distributions. The choice of the functional $\mathcal{J}$ is fundamental for the identification procedure to be successful. In this article, we use a functional based on the Error in the Constitutive Equation, which has important theoretical properties such as convexity [20]. One of the identification methods based on this functional is the Constitutive Equation Gap Method (CEGM), which has proven to be appropriate for material identification [15]. The functional used in the CEGM is

$$\mathcal{J}(E) = \min_{\sigma \in \mathcal{V}_\sigma} \mathcal{E}(\sigma, E) \; ; \; \mathcal{E}(\sigma, E) = \int_{\Omega} (\sigma - \mathbb{C}(E)\varepsilon) : \mathbb{C}(E)^{-1} (\sigma - \mathbb{C}(E)\varepsilon) \, d\Omega \tag{6}$$

where $\mathbb{C}(E) = E \, C_1$ is the constitutive tensor, C_1 is the constitutive tensor for $E = 1$, ε is the strain tensor, σ is the symmetric Cauchy stress tensor and $\mathcal{V}_\sigma$ is the set of admissible stress tensors. The regularization term considered is the Total Variation, which provides regularized material distributions without over-smoothing the solution [16].

3 RESULTS

3.1 Arterial lesion frames through the cardiac cycle

The aforementioned gating and registration stages of the methodology were applied to an in-vivo case. The IVUS study was acquired with the Atlantis® SR Pro Imaging Catheter 40 MHz

synchronized with an ECG signal and connected to an iLab™ Ultrasound Imaging System (both by Boston Scientific Corporation, Natick, MA, USA), at the Heart Institute (InCor), São Paulo, Brazil. A left anterior descending artery was imaged during automated pullback at 0.5 mm/s with a frame rate of 30 FPS, generating frames of 512 by 512 pixels with 17 μm of resolution. The procedure was performed during a diagnostic or therapeutic percutaneous coronary procedure.

After the acquisition, a specialist performed the segmentation of the R-wave peak along the ECG signal as explained in Section 2.1. From the gating of this study (see Figure 1), it is easily seen that the spatial description of the vessel is free of the saw-tooth artifact observed prior to the gating process. Thus, we obtain the vessel spatial description for different cardiac phases. Through these descriptions, we select a frame of interest (red arrow in Figure 1) and extract the associated cross-section in each cardiac phase by the axial registration process. As the structures are misaligned, we performed the registration proposed in Section 2.2. The result (Figure 2) is a set of frames at different cardiac phases in the same cross-section of the vessel, which describes the kinematics of the vessel wall without rigid motion after transversal registration stage.

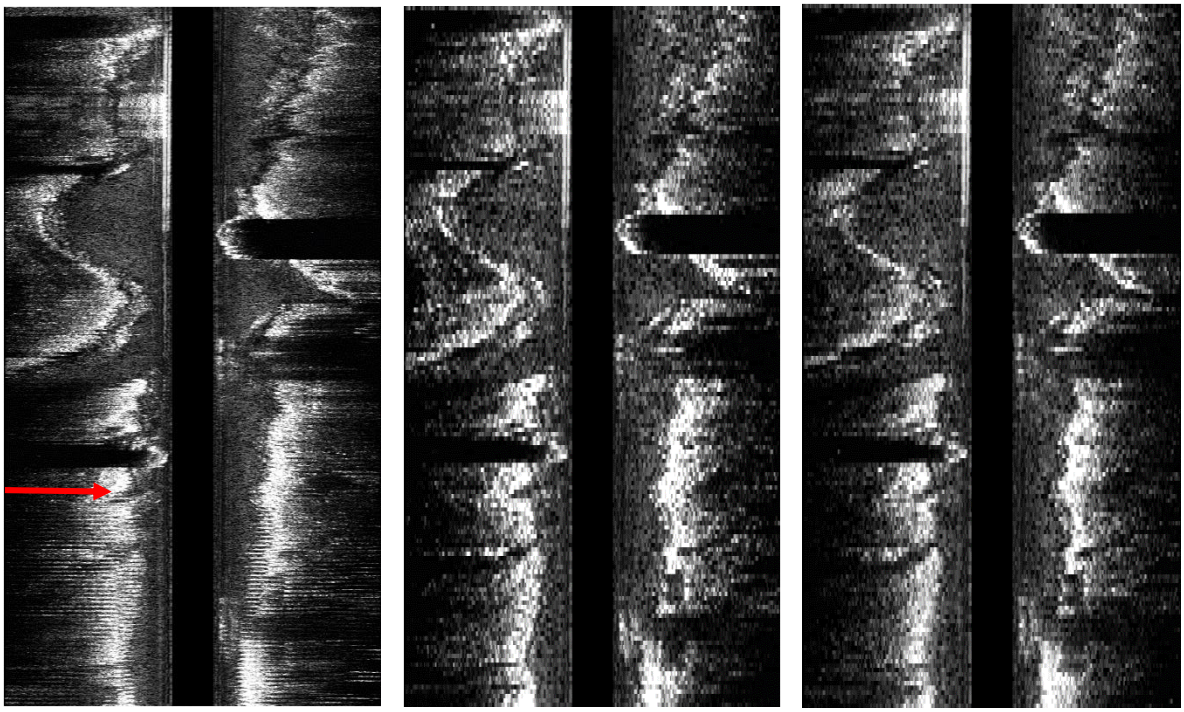

Figure 1: Longitudinal views of an in-vivo IVUS study: (left) before gating (red arrow depicting the place at which transversal registration is performed) ; (center) gating of $\Im_{st}$ cardiac phase; (right) gating of the 5th phase after $\Im_{st}$ phase (R-wave peak for this case).

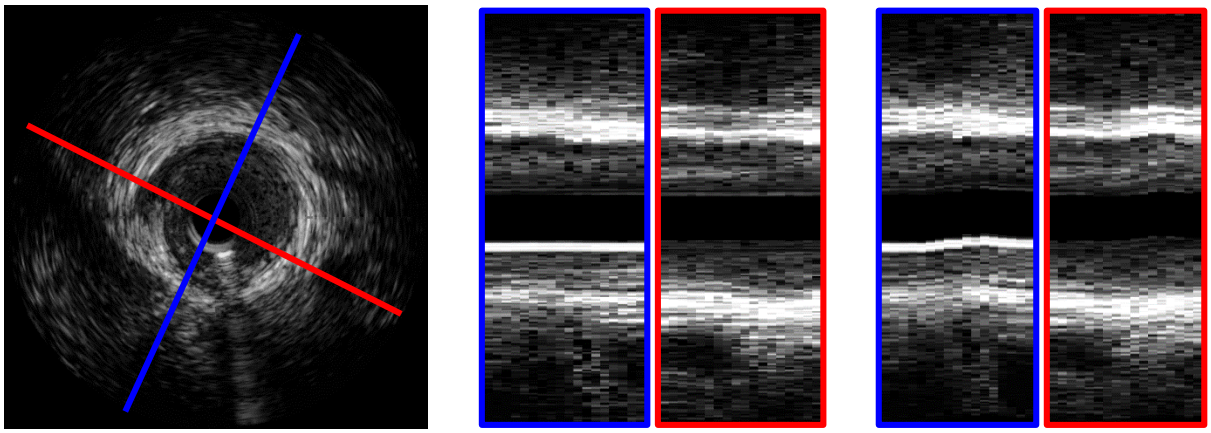

Figure 2: Results of the registration process of a frame of interest: (left) frame of interest at the $\Im_{st}$ phase depicting, in red and blue, the scan lines where the deformation is inspected along the cardiac phases; (center) deformation of the cross-section through the cardiac phases (from left to right) before registration; (right) deformation of the cross-section through the cardiac phases (from left to right) after registration.

3.2 Material parameter estimation in synthetic cases

To present the potentialities of the methodology presented in Sections 2.3 and 2.4, we proceed to estimate the material parameters for two different synthetic cases. In both of them, we only use two images (one before and one after deformation) and the forces applied at the boundaries are known. By using the images, we estimate the displacement field with the OF technique presented in Section 2.3. Afterwards, the obtained displacement field is used by the identification procedure, presented in Section 2.4, to estimate the material parameters.

3.2.1 Plate: uniaxial stress test

This test is usually considered in the material identification literature. Here, it is considered a square domain composed by a material with Young modulus $E_1 = 1 \cdot 10^6$ Pa with a rectangular inclusion of Young modulus $E_2 = 2 \cdot 10^6$ Pa at the center, both materials with Poisson ratio of $\nu = 0.3$. The applied loads are uniform tractions at the left and right boundaries of the domain. A more detailed description of the problem is presented in [14] as the Reference Problem 1.

Using Finite Element Method (FEM) (with a structured mesh of 1352 elements), we solve the linear elasticity problem with a known Young Moduli distribution. The displacement field obtained (see Figure 3.a, blue arrows) is used to generate the image after deformation for the OF problem. Then, we apply the OF method (see Equation (4)) with parameters $\beta_1 = 1 \cdot 10^4$; $\beta_2 = 1 \cdot 10^1$; $\rho = 1.6; \gamma = 1 \cdot 10^4$ obtaining the OF displacement field for the identification problem (see Figure 3.a, red arrows). The displacement field estimated by optical flow presents larger discrepancies over top and bottom boundaries due to the smooth constraints imposed by the regularization terms (see Figure 3.b).

Finally, the identification procedure fed by the OF displacements is employed with different values of the regularization coefficient α using the same mesh as in the FEM problem and estimating the Young Modulus at each element. The material distribution obtained for $\alpha = 2.4 \cdot 10^{-5}$ (see Figure 3.c) identifies clearly the squared inclusion. However, a stiffer material

appears on the top and bottom boundaries (see Figure 3.b) due to the underestimation performed by the OF (35% of error in the displacement field magnitude). By increasing the regularization coefficient to $\alpha = 1 \cdot 10^{-4}$, we obtain a distribution (see Figure 3.d) where the error in the top and bottom is reduced, and central inclusion is still identified. Although, the Young moduli values are less accurate due to the regularization in the identification process. From these results, it is seen that as the α value increases, we obtain a trade-off between the identification of the materials distribution and the accuracy in the estimation of material properties. It is important to highlight that mesh refinement improves the identification quality by localizing the errors, future work will consider this in order to avoid identifications errors overly spread in the solution.

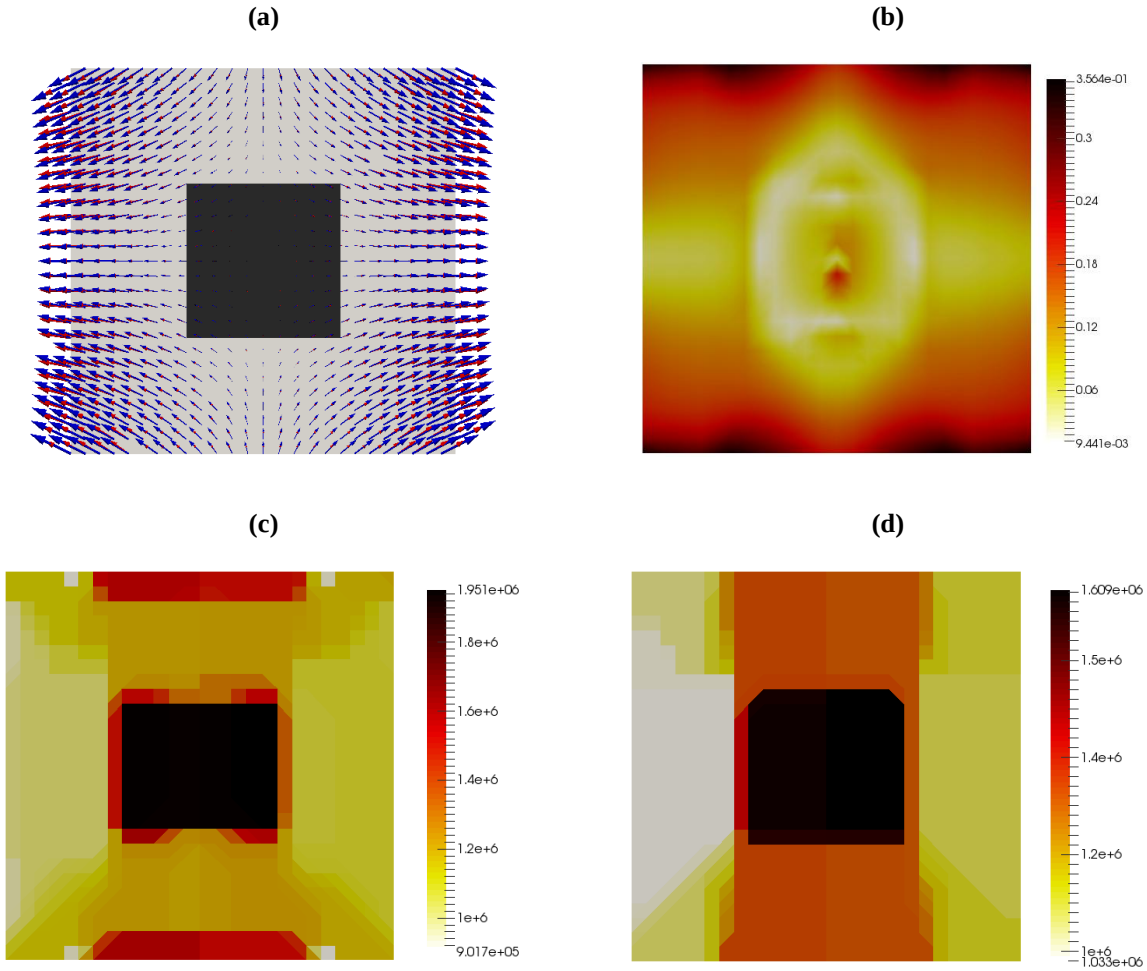

Figure 3: Plate uniaxial stress test: (a) Domain, its material distribution (light and dark gray present $E_1 = 1 \cdot 10^6$ Pa and $E_2 = 2 \cdot 10^6$ Pa, respectively), displacement field $\widehat{U}$ estimated by FEM (blue arrows) and displacement field U obtained by OF (red arrows); (b) relative error of the displacement field, ϵ_r, obtained by OF ($\epsilon_r = \|\widehat{U} - U\| / \|\widehat{U}\|$); (c) Young Modulus estimation for $\alpha = 2.4 \cdot 10^{-5}$; (d) Young Modulus estimation for $\alpha = 1 \cdot 10^{-4}$.

3.2.2 Ring: inflation test

An analogous procedure to Section 3.2.1 was followed using different geometry and loading conditions. We consider a ring composed by two materials submitted to an uniform internal pressure. A quarter of the ring is composed by a material with Young modulus $E_1 = 1 \cdot 10^5$ Pa while the remaining is formed by a material with Young modulus $E_2 = 6 \cdot 10^5$ Pa (light and dark gray materials in Figure 4.a), both materials with a Poisson ratio of $\nu = 0.45$.

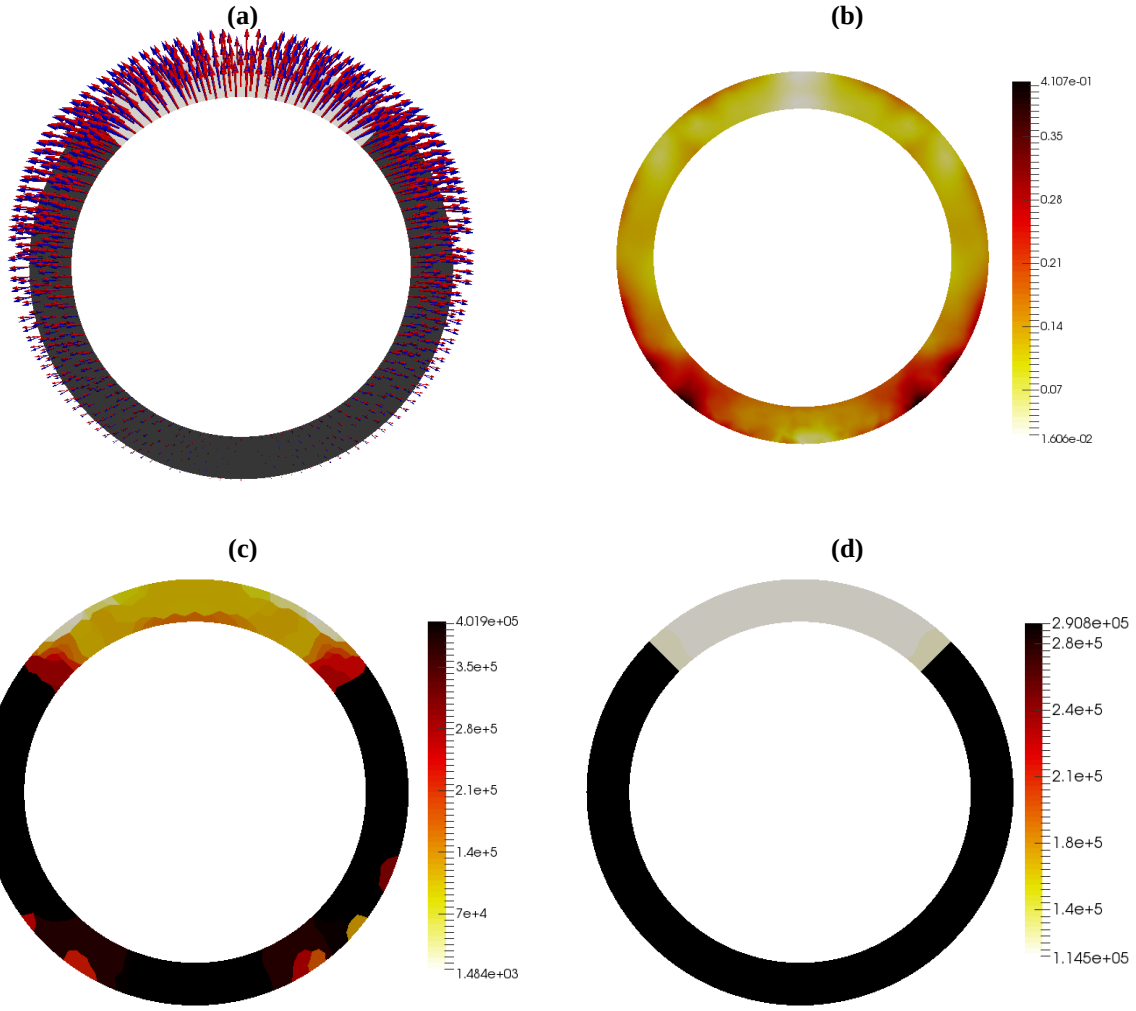

Figure 4: Ring inflation test: (a) Domain, its material distribution (light and dark gray present $E_1 = 1 \cdot 10^5$ Pa and $E_2 = 6 \cdot 10^5$ Pa, respectively), displacement field $\hat{U}$ estimated by FEM (blue arrows) and displacement field U obtained by OF (red arrows); (b) relative error of the displacement field, ϵ_r, obtained by OF ($\epsilon_r = \|\hat{U} - U\|/\|\hat{U}\|$); (c) Young Modulus estimation for $\alpha = 1.3 \cdot 10^{-4}$; (d) Young Modulus estimation for $\alpha = 3.1 \cdot 10^{-3}$.

As before, we solve the linear elasticity problem for the given Young Moduli distribution by using FEM, this time, with an unstructured grid of 1450 elements. The displacement field obtained (see Figure 4.a, blue arrows) is used to generate the image after deformation to feed

the OF problem and, afterwards, the OF method (see Equation (4)) with parameters $\beta_1 = 1 \cdot 10^4$; $\beta_2 = 1 \cdot 10^2$; $\rho = 6.4; \gamma = 5 \cdot 10^3$ is applied, obtaining the displacement field for the identification problem (see Figure 4.a, red arrows).

Finally the identification procedure is performed for two regularization coefficient values using the same mesh as in the FEM problem. Again, a smaller value of $\alpha = 1.3 \cdot 10^{-4}$ (see Figure 4.c) presents bigger error in areas associated with the bigger errors in the OF displacement estimation (see Figure 4.b). Then, a higher regularization factor, $\alpha = 3.1 \cdot 10^{-3}$ (see Figure 4.d) identifies clearly the morphology of the material distribution. As in the previous test, it is seen that lower values of α present a more accurate value of the Young Modulus distribution but also more sensitive to errors in the displacement field. As the value of α increases, the regularization decrease the Young Modulus of the materials and improves the characterization of material distribution.

5 CONCLUSIONS

The proposed methodology allows the extraction of a particular cross-section of the vessel along the cardiac cycle, removing the saw-tooth artifacts, spatial misalignments between the vessel structures and axial displacements of the transducer. The application of these pre-processing steps ease the visualization of the vessel wall strains, improving its assessment and, hence, allowing to classify the frames according to the pressure level associated with each cardiac phase.

Also, the bases for material parameter estimation for two synthetic cases were presented. The results show the correct identification of the materials distribution, which is key towards the successful characterization of the vessel mechanical properties. Hence, it was seen a trade-off between accurate identification of spatial distribution and accurate identification of the Young modulus values of the materials. A sufficiently small value of the regularization parameter delivers close values of the Young Modulus of materials with no displacement error in the OF displacement field. As the value of α increase, an accurate description of the material distribution is obtained but the Young Modulus values tend asymptotically to a mean Young Modulus of the solution, by the diffusive behavior of the regularization term.

Future work will focus on developing OF and identification methods robust enough to deal with the speckle noise presented in the IVUS studies. In this first study, it has been seen that the regularization of the identification process allows to recognize the materials distribution which would provide an important insight towards a refined search of the mechanical properties.

6 ACKNOWLEDGEMENTS

This research was partially supported by the Brazilian agencies CNPq, FAPERJ and CAPES and the Uruguayan agencies ANII and CSIC. The support of these agencies is gratefully acknowledged.

REFERENCES

[1] Naghavi, M., et al. From vulnerable plaque to vulnerable patient - Part III: Executive summary of the Screening for Heart Attack Prevention and Education (SHAPE) Task Force report. *Am J Cardiol* (2006) **98.2A**:2H–15H.

[2] Virmani, R., Burke, A.P., Farb, A., and Kolodgie, F.D. Pathology of the Vulnerable Plaque. *J Am Coll Cardiol* (2006) **47.8**:C13–C18.

[3] Nair, A., Kuban, B.D., Tuzcu, E.M., Schoenhagen, P., Nissen, S.E., Vince, D.G. Coronary plaque classification with intravascular ultrasound radiofrequency data analysis. *Circulation* (2002) **106**:2200–2206.

[4] Sathyanarayana, S., Carlier, S., Li, W., Thomas, L. Characterisation of atherosclerotic plaque by spectral similarity of radiofrequency intravascular ultrasound signals. *EuroIntervention* (2009) **5**:133–139.

[5] Kawasaki M, et al. In vivo quantitative tissue characterization of human coronary arterial plaques by use of integrated backscatter intravascular ultrasound and comparison with angioscopic findings. *Circulation* (2002) **105**:2487–2492.

[6] Ophir, J., Céspedes, I., Ponnekanti, H., Yazdi, Y., and Li, X. Elastography: A method for imaging the elasticity in biological tissues. *Ultrason Imag* (1991) **13**: 111–134.

[7] De Korte, C.L., et al. Characterization of plaque components and vulnerability with intravascular ultrasound elastography. *Phys Med Biol* (2000) **45.6**: 1465–1475.

[8] Schaar, J.A., et al. Characterizing vulnerable plaque features with intravascular elastography. *Circulation* (2003) **108.21**: 2636–41.

[9] Ciompi, F., Pujol, O., Gatta, C., Rodríguez-Leor, O., Mauri-Ferré, J., and Radeva, P. Fusing in-vitro and in-vivo intravascular ultrasound data for plaque characterization. *Int J Cardiovasc Imag* (2010) **26.7**: 763–779.

[10] Yamada, R., et al. A comparison between 40MHz intravascular ultrasound iMap imaging system and integrated backscatter intravascular ultrasound. *J Cardiol* (2012) **61.2**:149–154.

[11] Arbab-Zadeh, A., DeMaria, A.N., Penny, W.F., Russo, R.J., Kimura, B.J., and Bhargava, V. Axial movement of the intravascular ultrasound probe during the cardiac cycle: implications for three-dimensional reconstruction and measurements of coronary dimensions. *Am Heart J* (1999) **138.5 Pt 1**: 865–872.

[12] Bruhn, A., Weickert, J., and Schnörr, C. Lucas/Kanade meets Horn/Schunck: Combining local and global optic flow methods. *Int J Comput Vis* (2005) **61.3**: 211-231.

[13] Franquet, A., Avril, S., Le Riche, R. and Badel, P. Identification of heterogeneous elastic properties in stenosed arteries: a numerical plane strain study. *Comput Meth Biomech Biomed Eng* (2012) **15.1**:49–58.

[14] Florentin, E., Lubineau, G. Identification of the parameters of an elastic material model using the constitutive equation gap method. *Comput Mech* (2010) **46**:521–531.

[15] Geymonat, G., Pagano, S. Identification of mechanical properties by displacement field measurement: a variational approach. *Meccanica* (2003) **38**:535–545.

[16] Pérez Zerpa, J.M. *Caracterização de propriedades mecânicas em modelos de artérias usando um algoritmo de ponto interior*, MSc Dissertation, COPPE - Federal University of Rio de Janeiro, 2012.

[17] Zhu H. Retrieval of cardiac phase from ivus sequences. In: *Medical Imaging, International Society for Optics and Photonics* (2003): 135–146.

[18] O'Malley, S.M., Granada, J.F., Carlier, S., Naghavi, M., and Kakadiaris, I.A. Image-based gating of intravascular ultrasound pullback sequences. *IEEE Trans Inform Tech Biomed* (2008) **12.3**: 299–306.

[19] Hernandez-Sabate, A., Gil, D., Garcia-Barnes, J., and Marti, E. Image-based cardiac phase retrieval in intravascular ultrasound sequences. *IEEE Trans Ultrason Ferroelectrics Freq Contr* (2011) **58.1**: 60–72.

[20] Goenezen, S., Barbone, P., Oberai, A. Solution of the nonlinear elasticity imaging inverse problem: The incompressible case. *Comput Meth Appl Mech Eng* (2011):1406–1420.